GEOLOGICA CARPATHICA, 46, 2, BRATISLAVA, APRIL 1995
79 - 94

GRANITOID ALLANITE-(Ce): SUBSTITUTION RELATIONS, REDOX CONDITIONS AND REE DISTRIBUTIONS (ON AN EXAMPLE OF I-TYPE GRANITOIDS, WESTERN CARPATHIANS, SLOVAKIA)

IGOR PETRÍK[1], IGOR BROSKA[1], JOZEF LIPKA[2] and PAVOL SIMAN[3]

[1]Geological Institute, Slovak Academy of Sciences, Dúbravská cesta 9, 842 26 Bratislava, Slovak Republic
[2]Dept. of Nuclear Physics and Technique, Slovak Technical University, Ilkovičova 3, 812 19 Bratislava, Slovak Republic
[3]Dionýz Štúr Institute of Geology, Mlynská dolina 1, 817 04 Bratislava, Slovak Republic

(Manuscript received December 15, 1992; accepted in revised form December 13, 1994)

Abstract: Seven allanites-(Ce) from the Sihla type s.l., a characteristic I-type granitoid of the Western Carpathians, were studied in detail. The BSE images have revealed their internal zoning characterized by repeated interactions of primary grains with late- to postmagmatic fluids which produced a patchwork of domains of variable brightness. The microprobe - based study of substitution relations showed that allanite compositions are dominated by the substitutions $Ca + Fe^{3+} = Fe^{2+} + REE^{3+}$ (Fe-epidote-allanite) and $Ca + Al^{3+} = Fe^{2+} + REE^{3+}$ (Fe-epidote-ferriallanite). While bright domains are thought to be primary, the dark grey domains are interpreted as oxidated, the oxidation being compensated by partial REE escape. This interpretation is based on a new type of diagram (total REE+Th vs. Al) contoured with $F_{ox} = Fe^{3+}/(Fe^{3+} + Fe^{2+})$ isolines. The diagram enables a realistic estimation of the F_{ox} ratio of spot analyses of Fe-allanites as confirmed by Mössbauer-derived Fe^{3+}/Fe^{2+} ratios of two allanites. While igneous allanites seem to have F_{ox} ratios buffered at about 0.4, vein allanites are variably oxidated, and metamorphic allanites both oxidated and reduced. The distribution of LREE in allanites is characterized by Ce-dominance, the La/Nd ratio being rather low. The composition of the parental granitic liquid inferred from the compositions of the primary allanite domains and known LREE partitioning coefficients shows a strongly fractionated LREE distribution pattern.

Key words: Western Carpathians, granitoid rocks, Mössbauer spectroscopy, redox conditions, REE distributions, allanite-(Ce), Fe^{3+}/Fe^{2+} ratio.

Introduction

This work presents the chemical characterization of allanite-(Ce), the main carrier of light rare elements (LREE, RE in formulae), and a characteristic accessory mineral of Western Carpathian I-type granitoids. We discuss its internal zoning, substitution relations, Fe^{3+}/Fe^{2+} ratios in response to redox changes, and REE distributions, in view of primary and secondary processes.

In acidic magmas the REE typically form minerals of their own: monazite, allanite, xenotime. A substantial content of REE is also contained in other accessory minerals (titanite, apatite, zircon). Rock-forming biotite and hornblende contribute to granitoid rock budget generally by less than 20 % (e.g. Fourcade & Allegre 1978; Gromet & Silver 1983; Sawka & Chappell 1988). The main REE-minerals in the Variscan granitoids of the Western Carpathians are allanite and monazite (Hovorka 1960; Hovorka & Hvožďara 1965; Hovorka 1971; Hvožďara & Határ 1978; Broska & Uher 1991). The quantitative evaluation of their abundances in granitoids based on heavy fractions (Broska & Gregor 1992) showed that one of them always dominates over the other. Allanite-(Ce) was shown to be characteristic of the I-type granitoids which are represented by the regional type Sihla (s.l. Broska & Petrík 1993a). This rock type forms major parts of the granitic cores in the Western Carpathians (Petrík et al. 1994).

Allanite-(Ce), in contrast to monazite, is typically accompanied by magnetite. Based both on these features Broska & Gregor (l.c.) defined allanite-magnetite and monazite- ilmenite granitoid series. Recently, Petrík & Broska (1994) correlated the allanite and magnetite-bearing tonalites/granodiorites with the I-type, and monazite-bearing granites with the S-type of Chappell & White (1974).

Petrography

Characterized by the presence of tonalite/diorite microgranular enclaves (Petrík & Broska 1989; Broska & Petrík 1993b), the Sihla type s.l. is represented by medium grained biotite tonalite. The tonalite consists of following minerals:

Plagioclase (50-60 vol. %) is usually filled by sericite and clinozoisite, when preserved with maximum An_{45} in cores. Biotite (10-15 vol. %) is Mg-rich, often replaced by chlorite and/or epidote. Accessories (1-3 vol. %) are typically represented by abundant apatite, zircon, titanite, epidote, allanite, magnetite. K-feldspar and hornblende also occur in accessory amounts. Allanite-(Ce) (up to 0.25 vol. %) forms pleochroic sub- to anhedral grains, sometimes with visible internal zoning and often with epidote overgrowths. It typically occurs in aggregates with biotite or magnetite. On the basis of these microstructural fea-

tures, we consider it a primary magmatic mineral crystallizing in the main crystallization stage (see also the section: The REE distribution).

Two samples (*T88, ZK–83*), rich enough in allanite for separation, were measured by Mössbauer spectrometry. Both samples contain large allanite grains (0.7–3.6 mm in length) with complicated internal zoning (Figs. 1A–C, 3D). The sample *T88*, in addition, contains minute isometric allanite grains (size 150–300 μm) with relatively simple zoning: an inner bright phase is to a varying degree replaced by dark grey outer phases (Figs. 2A–D). The later phases cut (replace) irregularly the older, brighter phase suggesting a late-, or postmagmatic process. Microprobe analyses have confirmed that the bright phase is slightly enriched in total REE (≈23 wt. %) compared with darker phases (≈20 wt. %, Tabs. 3, 4).

In the biotite tonalites *ZK–83* and *T22* only large allanite grains (1800–3600 μm) were observed showing the most interesting internal structure. The *ZK–83* allanite (Figs. 1A, B) represents a mosaic formed of at least three phases with irregular, lobate contacts. The fourth, darkest phase replaces all others along rims and cracks. The formation of a dark rim along the broken grain suggests a late process which may have occurred after the solidification of magma. As in the sample T88, the differences between phases are due to the variable REE contents: the bright phase is richer in total REE.

The *T22* allanite (Fig. 1D) has the most complicated structure of all the studied grains. Cut perpendicularly to {010}, the grain displays a dark grey core overgrown by a euhedral light gray zone. The core preserves patches with distinct primary, oscillatory zoning, strongly damaged by later, darker replacement phases. A bright segment overgrowing crystal faces {100} and {110} of the darker internal core is significantly enriched in total RE_2O_3 (Tab. 1).

Both biotite tonalites *KMF–10* and *ZK–57* contain subhedral allanites up to 0.5 mm long with several zones of brightness (Figs. 3A, B) indicating more stages of replacement. Rich in accessories, biotite tonalite *ZK–12* (Cambel 1982) contains up to 1 mm long subhedral allanite grains almost completely replaced by darker phases often evolved along cracks and voids (Fig. 3C).

Whole rock petrochemistry (major, minor and trace element contents) and the overall petrology of the Sihla type s.l. tonalites are given in Broska & Petrík (1993a), *ZK* samples in Cambel (1982) and *VG* samples in Petrík et al. (1993) and *T* samples in Petrík & Broska (1994).

Sampling and methods

Seven samples of the Sihla type s.l. biotite tonalite were chosen for SEM and microprobe study of allanite:

1 - *T88A*, fresh biotite tonalite, village of Zlatno, rocky cliff, 2 km SW of the Javorový Hill, Tribeč Mts. **2** - Biotite tonalite *T22*, village of Kostoľany, the old quarry, Tribeč Mts. **3** - *KMF–10*, altered chlorite - epidote tonalite, Kunerád Valley, road cut, Malá Fatra Mts. **4** - *ZK–83* biotite tonalite, Sihla type s.s., village of Hriňová, the dam quarry, Slovenské Rudohorie (Vepor) Mts. **5** - *VG–13* biotite tonalite, rock cliffs on the E slope, S of the village of Hriňová, Slovenské Rudohorie (Vepor) Mts. **6** - *ZK–57*, biotite tonalite, village of Podkriváň, Sihla type s.s., Slovenské Rudohorie (Vepor) Mts. **7** - *ZK–12*, biotite tonalite Sopotnica Valley, Čierna Hora Mts.

Allanite-(Ce) (hereinafter called allanite) was analysed by electron microanalyser Jeol JCXA 733 Superprobe at accelerating voltage 20 kV using the following standards (C.M. Taylor): oxides for Ti, Mg, Al, Fe, Ce, Gd, wollastonite for Ca, Si, boride (LaB_6) for La. Synthetic glasses were used for Pr, Nd, Sm. The SEM backscattered electron image study was performed on the JEOL JSM 840 scanning electron microscope at 25 kV accelerating voltage (both at the Geological Institute of Dionýz Štúr, Bratislava). Both polished thin sections (T88, T22, ZK-83) and hand-picked allanite grains mounted in epoxy (T88, ZK-12, ZK-57, VG-13, KMF-10) were used for analytical and microscope work.

Because a substantial part of the iron in allanite may be in ferric form, the Fe^{3+}/Fe^{2+} ratio of T88 and ZK-83 allanites was determined by Mössbauer spectroscopy at the Department of Nuclear Physics and Technology, Slovak Technical University Bratislava. Pure mineral concentrates were obtained from crushed and ground rocks (aproximately 10 kg by weight) using the standard shaking table and heavy liquids technique. Mössbauer spectra were recorded at 512 channels with ^{57}Co (in Rh matrix) as a source (Kičinová 1992). Although the concentrates were hand-picked to get the highest purity, the Mössbauer spectra of the sample T88 revealed the presence of 5.5 % of Fe in magnetite which corresponds to ca. 2 % of magnetite in concentrate. This mineral was shown to occur typically with allanite in intergrowths (Fig. 2A of Petrík & Broska 1994). Similarly, epidote rims overgrowing some allanite grains may slightly increase the bulk Fe^{3+}/Fe^{2+} ratio.

In addition to allanite, biotite concentrates (ZK-83, T88) were obtained in a similar way and measured by Mössbauer spectrometry (Tab. 5).

Chemical variability of allanite

Structurally identical with epidote, allanite is a REE-containing mineral usually dominated by cerium. Depending on this element, a suffix can be added to its name, e.g. (Ce, La, Y), Levinson (1966). Its general formula may be written following Dollase (1971):

$$A_2 M_3 Si_3 O_{12} (OH)$$

with structural positions filled as follows:

$$A(1) = Ca$$

$$A(2) = Ca^{2+}, RE^{3+}, Th^{4+}, Sr^{2+}, Mn^{2+},$$

$$M(3) \text{ and } M(1) = Al^{3+}, Fe^{3+}, Fe^{2+}, Mn^{3+}, Th^{4+}, Mg^{2+}$$

$$M(2) = Al^{3+}$$

The three octahedral positions M(1)–M(3) differ in the arrangement of octahedra in single or multiple chains. The A(1), A(2) sites represent two polyhedra (cavities) between interconnected chains (Dollase 1971). The size of positions is in the following order:

$$M(3) > M(1) > M(2), \quad A(2) > A(1)$$

The major substitutions thus occur in the largest positions (l.c.). The allanite end-member containing only ferrous iron is:

$$Ca\ RE^{3+}Fe^{2+}Al\ AlSi_3O_{12}\ (OH)$$

In this case the exceeding charge carried by the RE^{3+} is compensated by substituting the ferric iron of the epidote structure by ferrous iron. It is a coupled substitution:

$$Ca^{2+} + Fe^{3+} = RE^{3+} + Fe^{2+} \qquad (1)$$

epidote allanite

Many other substitutions occur in allanite structure, e.g. $Al^{3+} = Fe^{3+}$, $Mg = Fe^{2+}$, Ca, OH = F (Serdyuchenko 1980; Peacor & Dunn 1988; Burt 1990).

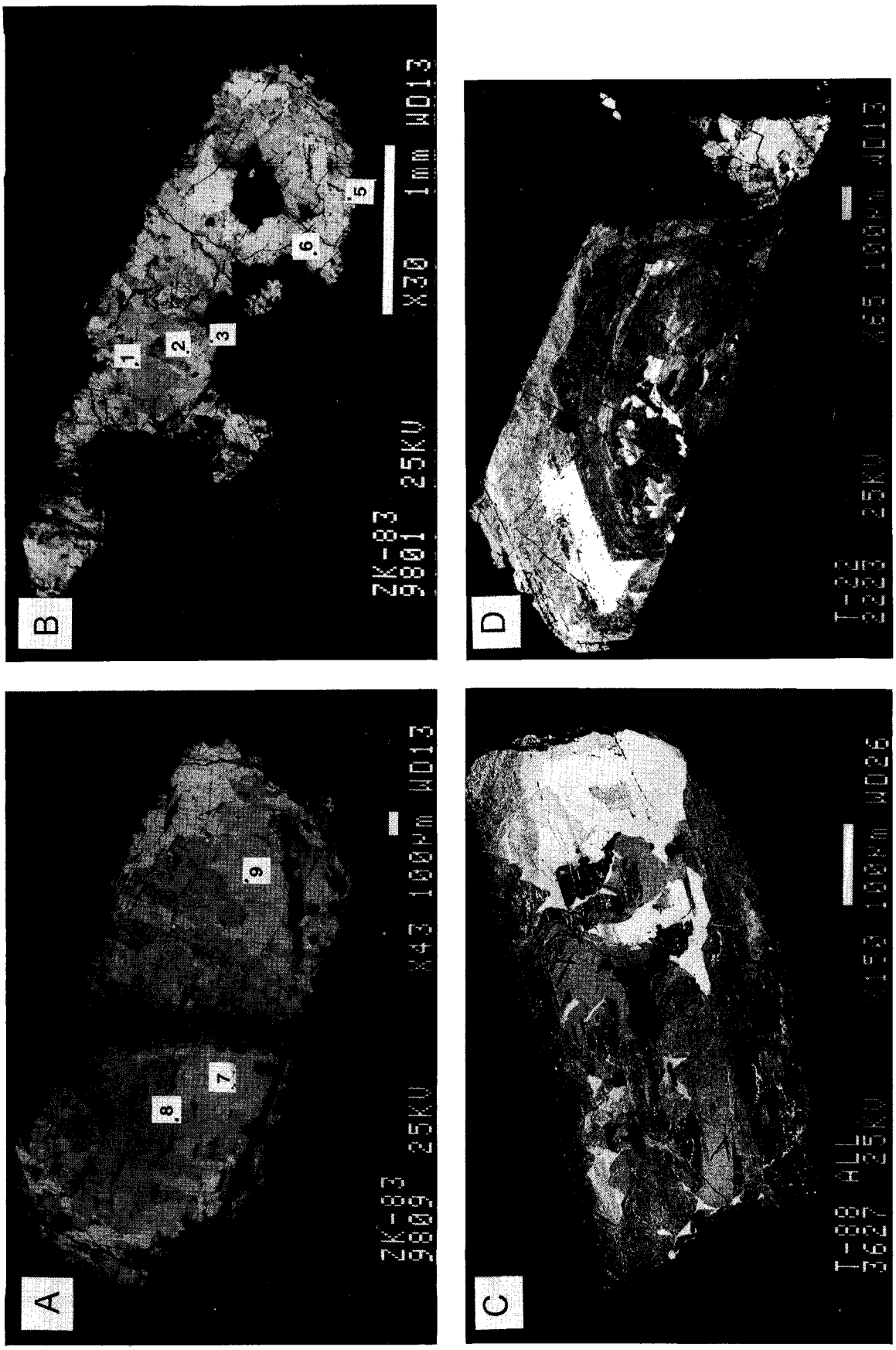

Fig. 1. Backscattered electron images of allanites ZK-83, T88. **A, B, C** – Large grains of the Sihla type tonalite showing a complicated history involving at least four phases. The numbered dots in A, B represent locations of the microprobe analyses given in Tab. 4. **D** – The most complicated allanite grain (Tribeč T22 tonalite) cut perpendicular to {010}, shows a euhedral shape. The brightest segment rimming euhedral core is markedly enriched in REE (Tab. 1).

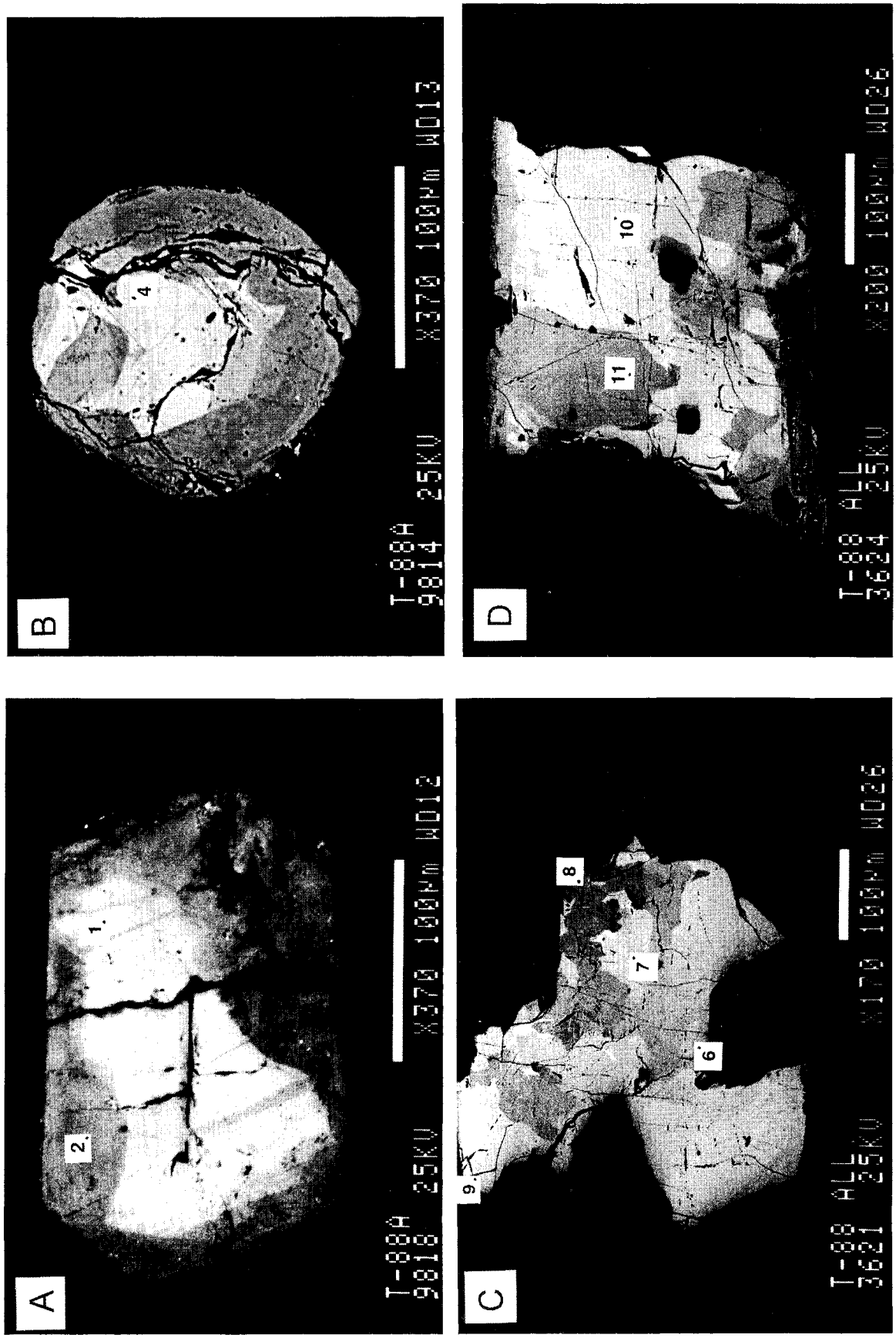

Fig. 2. Backscattered electron images of granitoid allanites T88: small size (**A**, **B**) and medium size (**C**, **D**) grains occur in Tribeč tonalite T88 together with large grains (Fig. 1C). Irregular darker phases apparently replace the primary brighter phase inward grain (A), along cracks (B) or around voids which served as fluid channels (D). The numbered dots represent locations of the microprobe analyses given in Tab. 3.

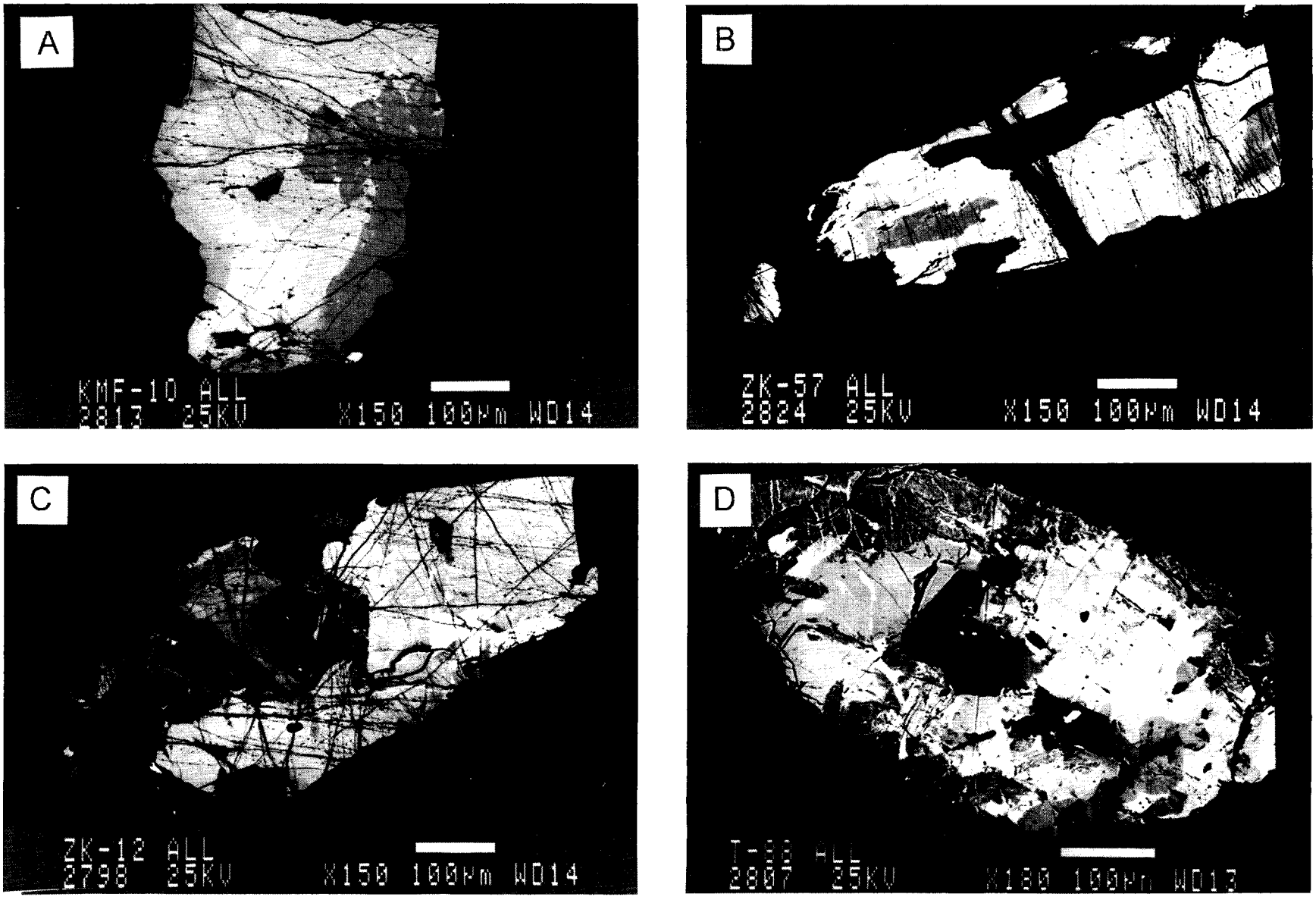

Fig. 3. Backscattered electron images of other studied allanites (KMF-10, ZK-57, ZK-12, T88) showing typical features of multiple replacement. All the grains display few remnants of a bright phase representing probably primary allanite composition.

Table 1: Mean microprobe analyses of allanites from the Malá Fatra (KMF-10), Čierna Hora (ZK-12), Vepor (VG-13, ZK-57) and Tribeč (T22) biotite tonalites (Sihla type s.l., Broska & Petrík 1993a).

Sample	KMF-10	ZK-12	VG-13	ZK-57	T22
n =	2	7	6	1	1
SiO_2	32.17	32.66	33.60	32.37	26.07
TiO_2	0.61	0.88	0.72	0.25	0.55
Al_2O_3	15.78	15.22	16.51	16.77	9.86
Fe_2O_3	5.71	3.95	4.56	0.22	6.04[1]
FeO	7.75	9.85	9.34	12.73	-
MgO	1.63	1.81	1.21	1.62	0.62
CaO	12.45	11.19	12.86	8.74	2.34
P_2O_5	0.00	0.00	0.02	0.09	0.00
La_2O_3	4.34	4.93	5.05	5.07	15.48
Ce_2O_3	11.19	12.12	11.13	13.06	26.19
Pr_2O_3	1.09	1.29	1.27	1.35	2.44
Nd_2O_3	3.07	3.02	1.99	4.00	3.12
Sm_2O_3	0.19	0.31	0.11	0.38	0.16
ThO_2	1.24	0.77	0.96	0.98	1.57
Total	97.22	97.60	99.33	97.63	94.44
Si	3.017	3.064	3.061	3.086	3.034
Ti	0.043	0.062	0.049	0.018	0.048
Al	1.744	1.682	1.773	1.884	1.353
Fe^{3+}	0.403	0.279	0.313	0.015	0.529[1]
Fe^{2+}	0.608	0.773	0.712	1.015	-
Mg	0.227	0.253	0.165	0.231	0.108
Ca	1.251	1.124	1.256	0.893	0.292
P	0.000	0.003	0.001	0.007	0.000
La	0.150	0.171	0.170	0.178	0.665
Ce	0.384	0.416	0.371	0.456	1.116
Pr	0.037	0.044	0.042	0.047	0.103
Nd	0.103	0.101	0.065	0.136	0.130
Sm	0.006	0.010	0.003	0.013	0.006
Gd	0.000	0.000	0.000	0.000	0.000
Th	0.026	0.016	0.020	0.021	0.042
Total	8.000	8.000	8.000	8.000	7.426
REE+Th	0.707	0.758	0.671	0.851	2.106
F_{ox}	0.399	0.256	0.305	0.015	-

Notes: Except T22, the formulae were recalculated to 12.5 oxygens and 8 cations with Fe^{3+}/Fe^{2+} balanced (after Droop 1987). $F_{ox}= Fe^{3+}/(Fe^{3+}+ Fe^{2+})$

n = number of spot analyses

[1]Total Fe as Fe_2O_3.

Table 2: Mean analyses of two allanites ZK-83 (Vepor Mts.) and T88 (Tribeč Mts.).

		ZK-83 n=8	T88 n=9	
SiO_2		32.98	32.05	
TiO_2		0.72	1.00	
Al_2O_3		15.87	15.08	
Fe_2O_3		5.79	7.69	
FeO		8.49	7.45	
MgO		1.25	1.43	
CaO		13.07	11.86	
P_2O_5		0.02	0.03	
La_2O_3		4.44	5.95	
Ce_2O_3		10.61	11.95	
Pr_2O_3		1.24	0.96	
Nd_2O_3		2.61	2.20	
Sm_2O_3		0.14	0.16	
Gd_2O_3		n.d.	0.19	
ThO_2		1.20	0.92	
Total		98.43	98.92	
T	Si	3.021	2.985	
M(1)	Ti	0.005	0.070	0.070
	Al	0.713	0.655	0.655
	Fe^{3+}	0.116	0.107	0.107
	Fe^{2+}	0.113	0.089	0.189[1]
	Total	0.992	0.921	1.021
M(2)	Al	1.000	1.000	
M(3)	Fe^{3+}	0.442	0.432	0.432
	Fe^{2+}	0.378	0.491	0.391[1]
	Mg	0.171	0.198	0.198
	Total	0.991	1.121	1.021
A(1)	Ca	1.000	1.000	
A(2)	Ca	0.283	0.183	
	P	0.001	0.002	
	La	0.151	0.204	
	Ce	0.358	0.408	
	Pr	0.042	0.033	
	Nd	0.086	0.073	
	Sm	0.005	0.005	
	Th	0.025	0.006	
	Gd	-	0.020	
	Total	0.951	0.934	
	Total cations	7.955	7.961	
	F_{ox}	0.532	0.482	

Notes: Structural formulae were calculated to 12.5 oxygens and total iron was divided into Fe^{3+} and Fe^{2+} in both M(1) and M(3) sites according to the Mössbauer data (Tab. 6). n - number of spot analyses
[1]0.1 atoms of Fe^{2+} shifted from M(3) to M(1) position. See text for details.

Chemical composition and substitutions

The chemical composition is presented in Tabs. 1-4: Mean analyses are given in Tabs. 1, 2 and spot analyses of the two samples studied in detail (T88, ZK-83) in Tabs. 3, 4. Besides the means, two spot analyses: the bright phase of the T22 sample (Fig. 1D) and the ZK-57 allanite having a slightly different composition (Fig. 8: the point near the 0.2 isoline) are given in the Tab. 1. The total FeO of the mean analyses (T88, ZK-83, Tab. 2) was partitioned according to Mössbauer-derived Fe^{3+}/Fe^{2+} ratios, while the other mean and spot analyses have structural formulae recalculated and iron divided according to the procedure of Droop (1987).

Inspection of the substitution relations of the studied allanites shows that the substitution (1) does not explain sufficiently the chemical variability of the allanites. Besides epidote ferric iron, the alumina is significantly replaced by ferrous iron to compensate the extra charge of the REE^{3+}:

$$Ca + Al^{3+} = RE^{3+} + Fe^{2+} \qquad (2)$$

The comparison of substitutions (1) and (2) provides the following scheme:

Substitution (1)	Substitution (2)
Epidote	*Epidote*
$Ca\,Ca\,Fe^{3+}Al\,AlSi_3O_{12}OH$	$Ca\,Ca\,Fe^{3+}\,Al\,AlSi_3O_{12}OH$
$Ca\,RE\,Fe^{2+}Al\,AlSi_3O_{12}OH$	$Ca\,RE\,Fe^{3+}\,Fe^{2+}AlSi_3O_{12}OH$
Allanite	*Ferriallanite*

While the substitution (1) results in theoretical Fe^{2+} allanite and epidote end-members, the equation (2) produces ferriallanite:

$$CaREFe^{3+}Fe^{2+}AlSi_3O_{12}OH.$$

The latter term is used by analogy with terms ferriannite, ferrimuscovite or ferriceladonite (e.g. Wones & Eugster 1965). The identical end-member was also suggested by Burt (1990). In natural allanites, Fe^{2+} is also substituted by Mg:

$$Fe^{2+} = Mg \qquad (3)$$

with dissakisite (or dollasite) end-member (Grew et al. 1991; Peacor & Dunn 1988).

The mean analyses of T88 and ZK-83 allanites (Tab. 2) have FeO_{tot} divided into Fe_2O_3 and FeO according to the obtained Mössbauer results (Tab. 6). Structural formulae were then calculated to 12.5 oxygens and cations divided after Dollase's (1971) suggestions for site-occupancy. The two analyses differ in the sum of octahedral cations, with the T88 allanite having an excess of 0.042 atoms pfu. While the ZK-83 allanite has nearly ideal filling of M positions, the T88 allanite shows an excess in M(3) position. Encountering the same problem, Dollase (1971) suggested that the separation precision of the Fe^{2+} between M(3) and M(1) position is low due to similar isomer shift and quadrupole splitting values and proposed to reduce the $Fe^{2+}_{M(3)}$ by 0.1 atom and to increase the $Fe^{2+}_{M(1)}$ by the same amount. This is done in Tab. 2 in the right column of T88 allanite. It is noteworthy that alumina in both allanites is accomodated only in M(2) and M(1) positions. Therefore, substitutions (1) and (2) may be written as follows:

$$Ca_{A(2)} + Fe^{3+}_{M(3)} = RE^{3+}_{A(2)} + Fe^{2+}_{M(3)} \qquad (1a)$$

$$Ca_{A(2)} + Al^{3+}_{M(1)} = RE^{3+}_{A(2)} + Fe^{2+}_{M(1)} \qquad (2a)$$

Redox conditions and the interpretation of allanite chemical variability

The plot REE vs. Al. The analysed allanites (T88, ZK-83) are shown in Fig. 4 together with the published data of Deer et al.

Table 3: Spot analyses of allanite T88.

Allanite T88									
Grain	1	1	2	3	3	3	3	4	4
Point	1	2	4	6	7	8	9	10	11
SiO_2	31.36	31.99	31.48	32.08	31.90	32.77	32.50	31.96	32.40
TiO_2	1.09	0.96	1.20	0.76	0.93	0.79	1.02	1.31	0.96
Al_2O_3	14.91	14.83	14.28	15.60	15.38	16.17	16.03	14.23	15.14
Fe_2O_3	6.69	3.33	4.33	7.60	6.57	7.33	5.88	5.40	6.40
FeO	8.43	10.20	10.43	7.87	8.46	7.75	9.38	9.76	8.90
MgO	1.61	1.26	1.83	1.23	1.35	1.04	1.46	1.65	1.40
CaO	11.63	11.36	10.02	12.88	12.25	13.62	11.77	11.10	12.10
P_2O_5	0.10	0.02	0.09	0.00	0.03	0.00	0.00	0.00	0.00
La_2O_3	5.15	6.80	5.34	6.05	6.57	5.74	6.65	5.25	5.97
Ce_2O_3	12.34	11.48	13.14	11.10	11.29	10.36	12.82	13.02	11.10
Pr_2O_3	1.26	0.77	1.18	0.75	0.82	0.73	0.99	1.12	1.03
Nd_2O_3	3.09	1.46	3.26	1.57	1.54	1.50	2.10	3.09	2.20
Sm_2O_3	0.28	0.08	0.28	0.00	0.10	0.07	0.13	0.32	0.08
Gd_2O_3	0.24	0.26	0.20	0.06	0.07	0.06	0.19	0.38	0.23
ThO_2	0.91	0.96	0.41	1.56	1.12	0.93	0.86	0.81	0.75
Total	99.09	95.76	97.57	99.11	98.38	98.86	100.78	99.40	99.66
O =					12.5				
Si	2.947	3.079	3.017	2.969	2.981	2.995	3.002	3.010	3.002
Ti	0.077	0.070	0.086	0.053	0.065	0.054	0.071	0.093	0.067
Al	1.653[1]	1.682	1.624	1.701	1.694	1.742	1.637	1.580	1.654
Fe^{3+}	0.473	0.241	0.313	0.529	0.462	0.504	0.409	0.383	0.447
Fe^{2+}	0.662	0.821	0.836	0.609	0.661	0.592	0.725	0.769	0.690
Mg	0.225	0.180	0.261	0.170	0.188	0.142	0.201	0.232	0.194
Ca	1.171	1.171	1.029	1.276	1.226	1.334	1.165	1.120	1.202
P	0.008	0.002	0.007	0.000	0.003	0.000	0.000	0.000	0.000
La	0.178	0.241	0.189	0.206	0.227	0.193	0.227	0.182	0.204
Ce	0.425	0.404	0.461	0.376	0.386	0.347	0.434	0.449	0.407
Pr	0.043	0.027	0.041	0.025	0.028	0.024	0.033	0.038	0.035
Nd	0.104	0.050	0.112	0.052	0.051	0.049	0.069	0.104	0.073
Sm	0.009	0.003	0.009	0.000	0.003	0.002	0.004	0.010	0.002
Gd	0.008	0.008	0.006	0.002	0.002	0.002	0.006	0.012	0.007
Th	0.019	0.021	0.009	0.033	0.024	0.019	0.018	0.017	0.016
Total	8.000	8.000	8.000	8.000	8.000	8.000	8.000	8.000	8.000
REE+Th	0.786	0.755	0.827	0.694	0.721	0.637	0.791	0.813	0.744
F_{ox}	0.417	0.227	0.272	0.465	0.411	0.460	0.361	0.332	0.393

Notes: Numbers refer to the locations shown in Fig. 2. See also notes to Tab. 1.

Table 4: Spot analyses of allanite ZK-83.

Allanite ZK-83								
Grain	1	1	1	1	1	2	2	2
Point	1	2	3	5	6	7	8	9
SiO_2	33.39	32.79	33.57	33.37	32.11	32.97	33.33	32.30
TiO_2	0.49	0.78	0.54	0.75	1.06	0.76	0.65	0.75
Al_2O_3	16.96	15.77	16.19	16.00	14.04	15.88	16.43	15.69
Fe_2O_3	5.22	5.57	6.77	5.11	4.62	6.06	6.47	6.52
FeO	8.55	8.52	7.78	9.17	9.60	8.25	8.06	7.93
MgO	0.85	1.24	0.98	1.23	2.03	1.32	1.09	1.28
CaO	13.81	12.92	14.28	12.98	10.77	13.10	13.78	12.94
P_2O_5	0.00	0.02	0.00	0.04	0.03	0.00	0.00	0.00
La_2O_3	4.18	3.92	4.51	3.91	5.59	4.13	5.12	4.12
Ce_2O_3	9.20	10.65	9.69	10.41	13.33	10.81	10.09	10.68
Pr_2O_3	0.98	1.44	1.16	1.27	1.51	1.28	1.01	1.28
Nd_2O_3	1.82	3.07	1.94	3.05	3.05	3.10	1.64	3.23
Sm_2O_3	0.07	0.22	0.00	0.15	0.09	0.18	0.00	0.00
ThO_2	1.55	0.82	1.32	1.38	0.79	1.08	1.36	1.28
Total	97.07	97.73	98.73	98.82	98.62	98.92	99.03	98.00
O =				12.5				
Si	3.064	3.042	3.050	3.060	3.046	3.029	3.029	3.004
Ti	0.034	0.054	0.037	0.052	0.076	0.053	0.044	0.052
Al	1.834	1.724	1.734	1.729	1.569	1.719	1.760	1.720
Fe^{3+}	0.361.	0.389	0.463	0.353	0.330	0.419	0.443	0.457
Fe^{2+}	0.656	0.661	0.591	0.703	0.762	0.634	0.612	0.617
Mg	0.116	0.172	0.133	0.168	0.287	0.181	0.148	0.177
Ca	1.358	1.284	1.390	1.275	1.094	1.289	1.342	1.290
P	0.000	0.002	0.000	0.003	0.002	0.000	0.000	0.000
La	0.141	0.134	0.151	0.132	0.196	0.140	0.172	0.141
Ce	0.309	0.362	0.322	0.349	0.463	0.364	0.336	0.364
Pr	0.033	0.049	0.038	0.042	0.052	0.043	0.033	0.043
Nd	0.060	0.102	0.063	0.100	0.103	0.102	0.053	0.107
Sm	0.002	0.007	0.000	0.005	0.003	0.006	0.000	0.000
Th	0.032	0.017	0.027	0.029	0.017	0.023	0.028	0.027
Total	8.000	8.000	8.000	8.000	8.000	8.000	8.000	8.000
REE+Th	0.577	0.671	0.601	0.657	0.834	0.678	0.622	0.682
F_{ox}	0.355	0.370	0.439	0.334	0.302	0.398	0.420	0.426

Notes: Numbers refer to the locations shown in Fig. 1. See also notes to Tab. 1.

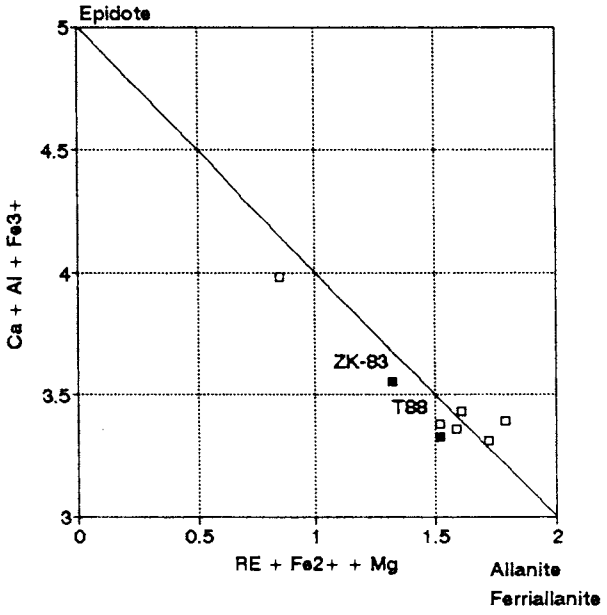

Fig. 4. Allanite compositions with determined Fe^{3+}/Fe^{2+} ratio related to the coupled substitution epidote - allanite, ferriallanite (5). Additional data from Deer et al. (1962), and Čech et al. (1972) are shown together with T88A and ZK-83 allanites.

(1962), analyses 8, 9, 11, 12, Dollase (1971), and Čech et al. (1972). The data seem to follow the line of the substitutions (1, 2, 3). However, the use of Fe^{3+} and Fe^{2+} in the plot excludes a great number of published allanite microprobe analyses reporting only FeO_{tot}. Indeed, there is a lack of allanite analyses with reliably determined Fe^{3+}/Fe^{2+} ratios most of them being of older date. Therefore, a plot expressing the substitutions (1, 2) is suggested, which avoids the use of Fe^{3+} and Fe^{2+}: total REE (+ other A(2) site cations except Ca) vs. Al (Fig. 5). In this plot epidote, allanite, ferriallanite and clinozoisite form apices of a quadrangle. Since the charge-balanced equations (1, 2) enable a unique determination of the ratio $F_{ox} = Fe^{3+}/(Fe^{3+} + Fe^{2+})$, isolines of this ratio may have been superimposed over the plot in Fig. 5. Spot analyses of allanites T88 and ZK-83 (Tab. 3, 4) are plotted in Figs. 6, 7. The point numbers in the tables refer to those in the figures. Projection points lie between the substitution lines epidote - allanite (1) and epidote - ferriallanite (2). A remarkable feature of the plot is that allanite compositions seem to parallel the substitution (2) but are displaced to the allanite apex.

I-type granite allanites. Also shown in Figs. 6 and 7 are the mean analyses (T88 and ZK-83) with Mössbauer- derived F_{ox} ratios (squares). The dark, grey and open symbols refer to dark, grey and bright phases of allanites (Figs. 1A-B, 2A-D), respectively. The trends of spot analyses cut isolines 0.4-0.5 at a low angle. While the dark grey phases (Figs. 6, 7) are displaced towards higher values of $F_{ox} = 0.5$, the bright phases are located close to the $F_{ox} = 0.40$ isoline. Mössbauer-derived ratios ($F_{ox} = 0.48$ in T88A and 0.53 in ZK-83, Tab. 6) agree well with the positions of means (squares) relative to F_{ox} isolines. The plot not only distinguishes between the higher oxidation state of ZK-83 allanite compared to T88 allanite but makes it possible to interpret the difference between bright (primary) and dark (secondary) domains of the allanites in terms of oxidation/reduction. The bright patches, which possibly represent remnants of primary allanites (Figs. 1-3), may be interpreted as having preserved original non-oxidized F_{ox} ratio (≈0.4). Various dark grey domains were later oxidated to values $F_{ox} > 0.5$ with the compensating escape of a part of REE. As darker domains are typically developed along cracks, voids and rims (Figs. 1-3), they may be interpreted as resulting from multiple interactions of primary allanite with late-stage oxidizing fluids.

Some analyses (epidote KMF-10, Fig. 8) suggest that the process reached a complete substitution of allanite by Al- Fe epidote with F_{ox} close to 1. However, this epidote represents epitaxial rim rather than original allanite replaced by epidote. The complete transition allanite - epidote is, therefore, not documented in the Western Carpathian I-type granitoids. The low REE analyses of Exley (1980), and Sorensen (1991) (Fig. 9) refer, respectively, to rims and hydrothermal veins, or metasomatically altered metamorphic allanites.

The bright segment of T22 allanite (Fig. 1D, Tab. 1) has doubled RE_2O_3 contents. Zakrzewski et al. (1992) observed similar zones in magnesian allanites-(Ce) and interpreted them as a mixture of bastnäsite and allanite. In our case the analysis

Table 5: Comparison of Mössbauer-derived Fe^{2+} and Fe^{3+} for allanites and biotites (in atom. %).

Sample	T88		ZK-83	
Mineral	allanite	biotite	allanite	biotite
Fe^{3+}	48.15	15.7	53.2	12.3
Fe^{2+}	51.85	84.3	46.8	87.7

Table 6: Mössbauer parameters of two measured allanites.

	$Fe^{2+}M(3)$			$Fe^{2+}M(1)$		
	IS	QS	Area	IS	QS	Area
	mm/s	mm/s	%	mm/s	mm/s	%
T88[1]	0.97	1.65	41.5	1.10	1.92	7.5
ZK-83	0.97	1.64	36.0	1.07	2.00	10.8
	$Fe^{3+}M(3)$			$Fe^{3+}M(1)$		
	IS	QS	Area	IS	QS	Area
	mm/s	mm/s	%	mm/s	mm/s	%
T88[1]	0.26	2.00	36.5	0.24	1.07	9.0
ZK-83	0.26	1.99	42.1	0.25	1.10	11.1

Notes: IS - isomer shift, QS - quadrupole splitting, M(1), M(3) - different octahedral positions of Fe. Error according to subspectral areas is ±1.5%.
[1]T88 contains 5.5 % of Fe in magnetite

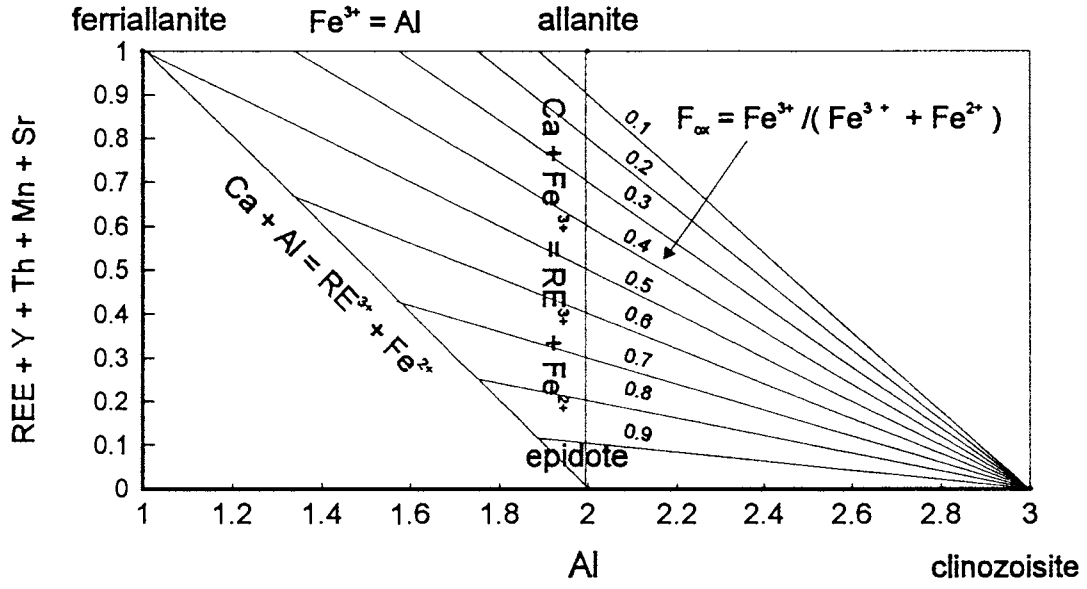

Fig. 5. The plot: total REE + Th + Mn + Sr (i.e. A(2) site cations except Ca) vs. Al contoured with isolines of the ratio $F_{ox} = Fe^{3+}/(Fe^{3+} + Fe^{2+})$ illustrating substitutions (1): allanite - epidote, (2): ferriallanite - epidote, and Fe^{3+} = Al: ferriallanite - allanite.

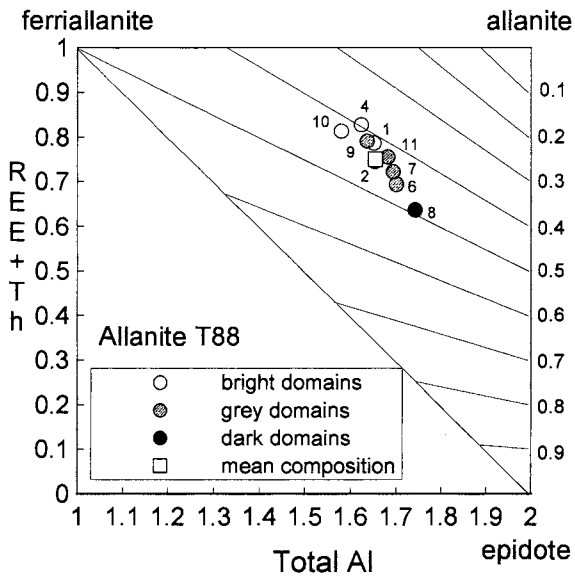

Fig. 6. Substitutions in T88 allanite spot analyses (Tab. 3) compared with F_{ox} isolines (right-hand column numbers refer to F_{ox} values). Various shades approximately correspond to bright, grey and dark domains (Fig. 2). The square is a mean analysis with Mössbauer-derived F_{ox} = 0.48.

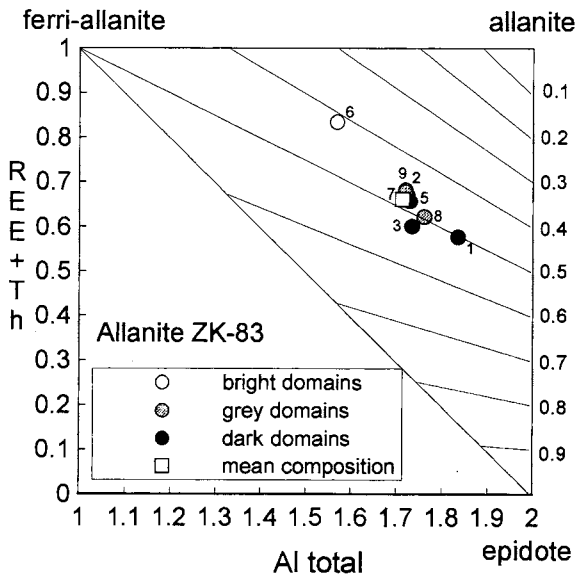

Fig. 7. Substitutions in ZK-83 allanite spot analyses (Tab. 4) compared with F_{ox} isolines. The square is a mean analysis with Mössbauer-derived F_{ox} = 0.53. Symbols as in Fig. 6.

total seems to be too high (94.4 %) for such an interpretation, and we tentatively suggest that the high mean atomic number area may have formed due to re-precipitation of the REEs mobilized from the dark patches in the core. A simple cerium-based mass balance would show that at the difference 3.5 wt. % between primary and depleted domains, a mass of primary allanite 5× larger than the enriched segment would have produced the required amount of Ce_2O_3 (26.19 %).

Redox conditions in parental magma and comparison with biotite. Primary allanites (persisting bright domains, Figs. 1-3, open circles in Figs. 6, 7) seem to fall approximately on the F_{ox} = 0.4 isoline as do other igneous allanites in Fig. 9 (open symbols). Therefore, it seems possible to interpret igneous allanite compositions as being buffered at a constant oxygen fugacity. As allanite itself is probably not a member of a buffering assemblage, the F_{ox} ratios of primary allanite domains may have resulted from the equilibration with biotite. Biotite together with magnetite and K-feldspar buffers fO_2 in granitoid magmas (Wones & Eugster 1965).

The comparison of Mössbauer-derived F_{ox} ratios of biotites coexisting with allanites (T88, ZK-83, Tab. 5) shows that biotite F_{ox} values do not correlate directly with those of allanite.

However, as argued above, the primary allanites converge to the value F_{ox} = 0.4. This value, rather than Mössbauer data including late-stage oxidation effects, is believed to indicate an equilibrium with biotite. Actually, the available biotite Möss-

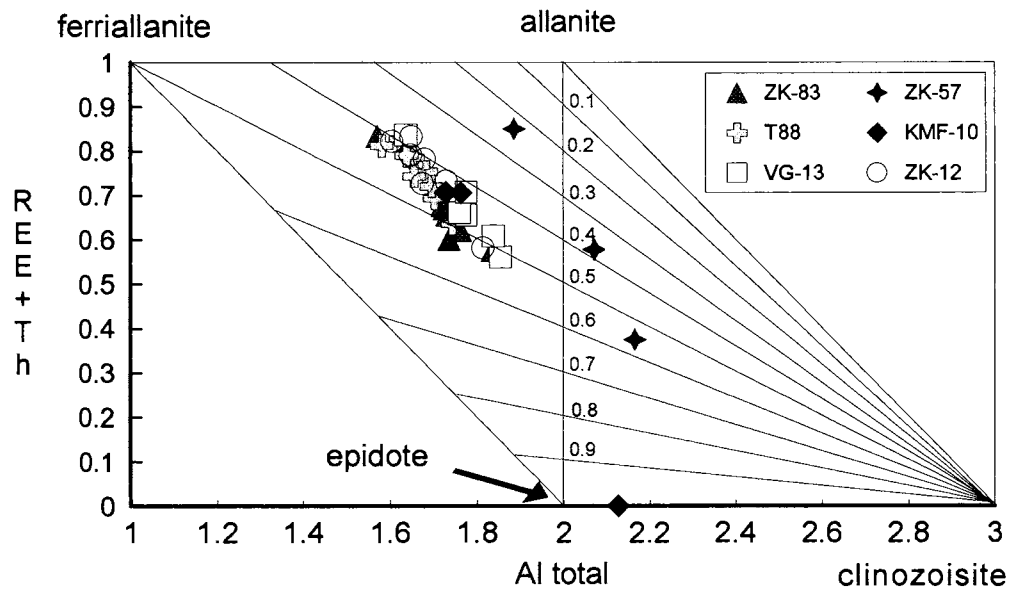

Fig. 8. Allanite compositions (spot analyses) of all six studied I-type tonalites T88, ZK-83, VG-13, ZK-57, KMF-10 and ZK-12. The low REE point of KMF-10 represents epitaxial epidote rim.

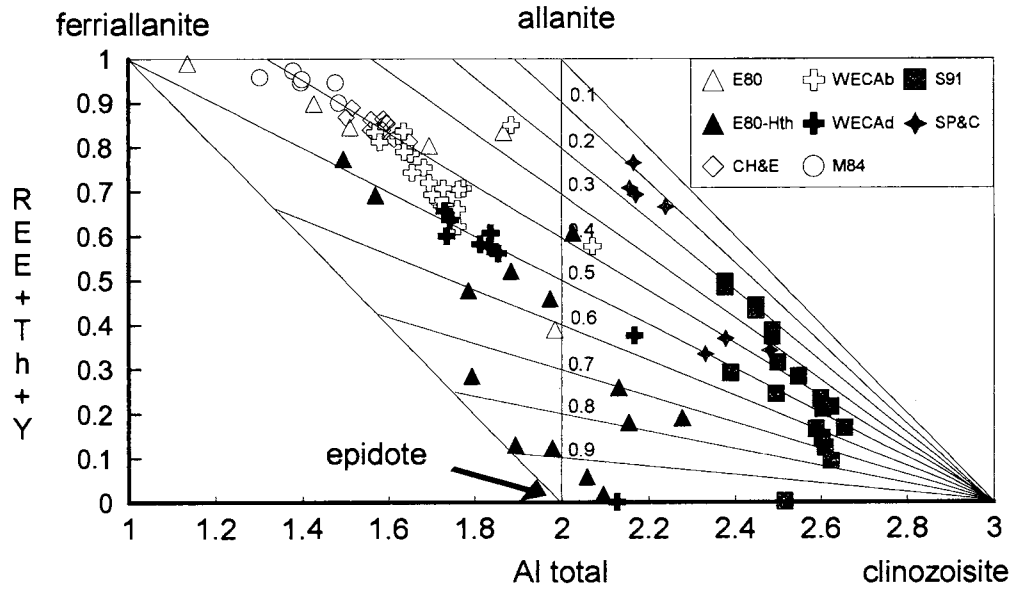

Fig. 9. Western Carpathian allanite data compared with published allanites from various mineral assemblages. Open, grey and black symbols refer to igneous, metamorphic and post-magmatic allanite compositions, respectively. E80 and E80-Hth: Exley (1980) igneous and vein allanites, respectively, CH&E: Chesner & Ettlinger (1989), M84: Michael (1984), S91: Sorensen (1991), SP&C (Spišiak et al. 1994), WECAb and WECAd: Western Carpathians, bright and dark domains, respectively.

bauer data (Petrík, Lipka in prep.) show a rather narrow range in F_{ox} values (0.12–0.17) for biotites along much of the Western Carpathian I-type granite belt. This is interpreted as due to biotite being buffered at oxygen fugacity which may be approximated e.g. by TMQA buffer (Noyes et al. 1983).

Oxidation or REE leaching? The oxidation character of late- to post-magmatic processes in I-type granitoids is documented by titanite and Fe-Ti oxides. Late, anhedral titanite which often occurs with pure magnetite grains indicating high fO_2 conditions is characteristic of the I-type tonalites. The process may well also be responsible for the partial oxidation of the allanite, the late titanite being a possible sink for mobilized REEs. We, therefore, consider the oxidation, rather than REE leaching, to be the primary cause of substitution processes in the allanites. Unlike the primary allanites, late- to post- magmatic allanite domains and rims, as well as vein allanites, do not seem to have been buffered (Fig. 9).

Estimation of the Fe^{3+}/Fe^{2+} ratio. As the plot suggested in Figs. 5–9 gives an independent possibility of estimating the amount of Fe^{3+}, a comparison with stoichiometric calculations would be of interest. This is possible because all the analyses in Figs. 6–9 and Tabs. 1, 3, 4 have iron partitioned according to the charge-balance criterion for a fixed number of negative charges (Droop 1987). The comparison shows that the F_{ox} values based on this equation (l.c.) are systematically lower than those read off the plot, Figs. 6–9. The discrepances between the two meth-

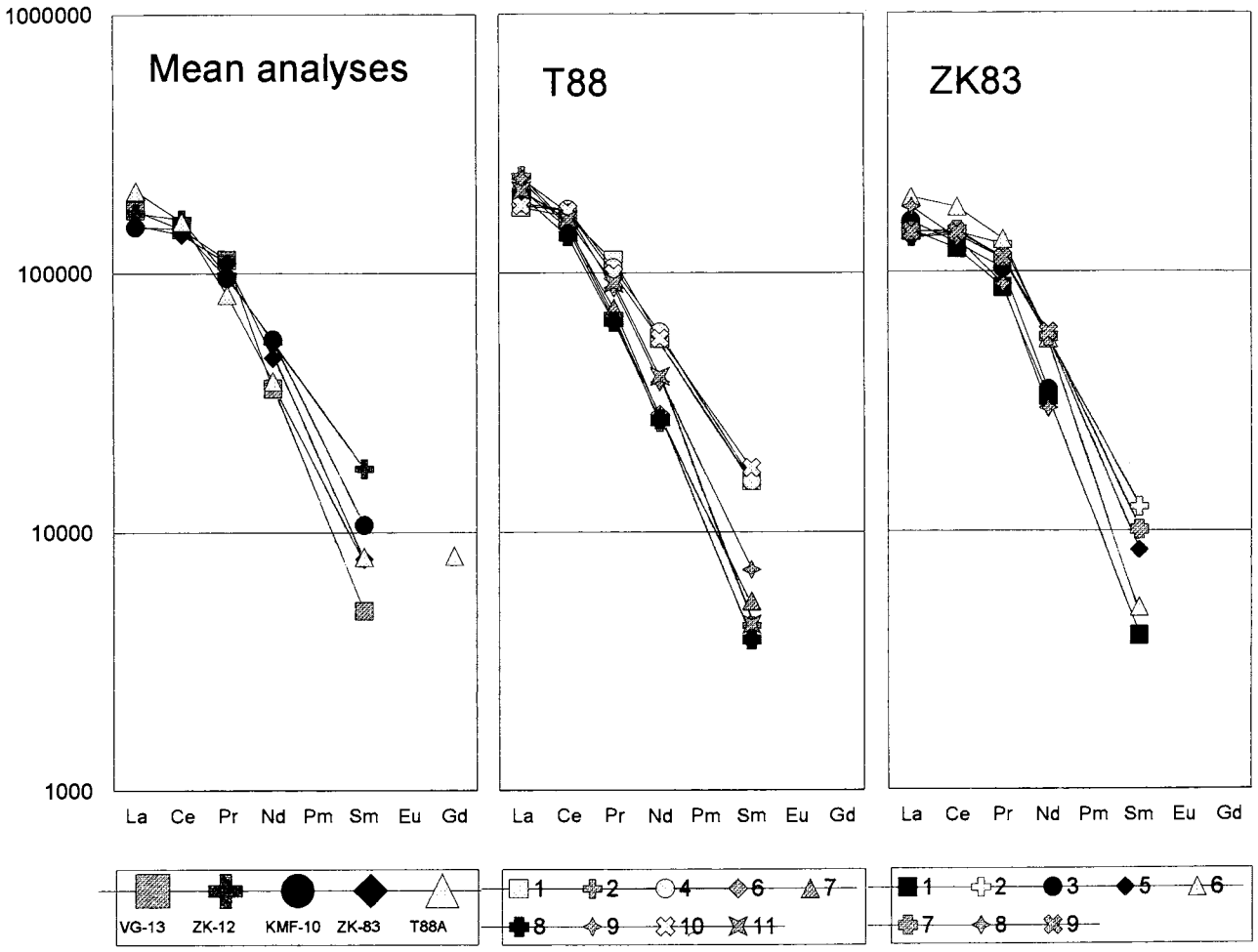

Fig. 10. The chondrite-normalized LREE distribution patterns of five mean allanite analyses of the studied I-type tonalites compared with spot analyses of T88 and ZK-83 allanites. Shades of symbols approximately correspond to brightness of analysed domains. Numbers of spot analyses refer to Figs. 1, 2, 6, 7 and Tables 3, 4.

ods result from vacancies in the A(2) site shown by most analyses. This is also documented by the excess of Si and octahedral cations (Al, Ti Fe, Mg) which balance the deficiency of A(2) site cations. The presence of vacancies violates the assumptions of Droop (1987) and actually means that the calculated values represent the lower limit of the F_{ox} ratio. Similarly, the excess of A-site cations would cause the overestimation of this ratio. A plot of the type: 2-Ca (instead of REE) vs. 3-Fe_{tot} (instead of Al) would yield F_{ox} values much more similar to those given by Droop's equation. However, the fact that the diagram (Figs. 5-9) includes only the cations really involved in the substitutions (1, 2) makes the F_{ox} values read off the plot more realistic. This is unequivocally confirmed by Mössbauer spectrometry (Tab. 6).

Comparison with other allanites

A number of Mg- and Mn-poor igneous, metamorphic and hydrothermal allanites are shown in Fig. 9. The analyses cover almost the whole area of the quadrangle: ferriallanite-allanite-clinozoisite-epidote. While the igneous and hydrothermal allanites (Exley 1980; Michael 1984; Chesner & Ettlinger 1989; this work) are displaced to the Al-poor part of the quadrangle, those of the metamorphic Al-rich, phengite- and corundum-bearing rocks of Sorensen (1991) and Spišiak et al. (1994), plot close to the allanite-clinozoisite join. Both groups are characterized by a compositional change from allanite-ferriallanite to epidote-clinozoisite join, with more or less pronounced concomitant increase of F_{ox}. However, the group of igneous allanites (Fig. 9, open symbols) forms a distinct belt along the F_{ox} = 0.4-0.5 corroborating the above assumption on the buffered nature of granitoid allanite. Indeed, ca. 40 % of ferric iron seems to be characteristic of the primary allanites coexisting with magnetite from I-type granite magmas reflecting relatively high oxygen fugacity during crystallization. The most reduced is a group of metamorphic allanites with the highest REE contents (F_{ox} = 0.1-0.2) coexisting with corrundum and phlogopite (Spišiak et al. 1994). The most oxidized are late hydrothermal (vein) and metamorphic minerals which correspond rather to REE enriched epidote - clinozoisite than to allanite.

The REE distribution

Allanite has a characteristic REE distribution pattern with strongly dominating light REE and commonly with negative Eu anomaly (Čech et al. 1972, Fourcade & Allégre 1978, Gromet & Silver 1983, Chesner & Ettlinger 1989). The LREE distribution patterns of 5 mean allanites are shown in Fig. 10 together with spot analyses of T88 and ZK-83. Western Carpathian granitoid allanites are generally comparable with other granitoids and acid volcanics (l.c.). The prevalence of Ce over La (La_N/Nd_N

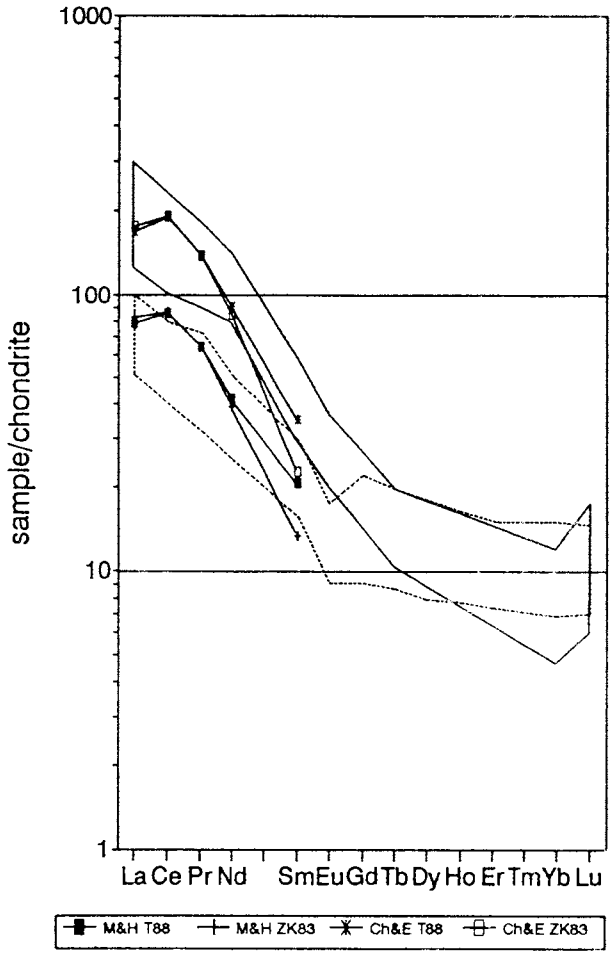

Fig. 11. Compositions of parental granitoid magma calculated using two sets of partition coefficients: M&H (Mahood & Hildreth 1983), Ch&E (Chesner & Ettlinger 1989) and primary allanite analyses (bright domains of T88, ZK83). The solid line field: Western Carpathian I-type granitoids, the dashed line field: continental arc turbidites (McLennan 1990).

ratio ≈2.5–4, Tabs. 1, 2) determines the cerium type of allanite. This ratio is significantly lower in comparison with allanites-(La) which have La_N/Nd_N of about 13–50 (e.g. Sawka et al. 1984 and Sawka & Chappell 1988).

Various shades in Fig. 10 (ZK-83 and T88) correspond approximately to the various brightness of analysed domains (Figs. 1, 2). The numbers of analyses refer to those in Figs. 1, 2 and 6, 7. As expected, the dark, oxidized domains (dark grey symbols) define the low LREE boundary of T88 and ZK-83 allanite fields. The depletion seems to be more effective for middle REEs with a slight, concomitant rise of the La/Ce ratio. A similar pattern of LREE decrease in zoned allanite, observed by Sawka et al. (1984), was interpreted as being primary, due to reduced partitioning coefficients. In contrast, on the basis of observation of the textural relations of various brightness domains, we prefer a post-magmatic origin of the dark domains. Indeed, a detailed study of allanite BSE images appears to be a pre-requisite for any interpretation of the allanite zoning. The interaction of primary allanites with late-stage fluids results in both oxidation and REE mobilization. However, the degree of this mobility is low: if the dark domains formed 50 % of allanite volume, the concentration difference between bright and dark domains was 42700 ppm of LREE (La to Gd), the mass of allanite 0.3 %, the successful escape of LREE from allanite would decrease a typical whole rock LREE content 350 ppm by 18 %.

As mentioned in the section on Petrography, we consider allanite a primary phase. This is in contrast with Hovorka (1971), who suggested an Alpine origin of allanite, but in accord with the older interpretation of Hovorka & Hvoždara (1965). Allanite crystallizes together with biotite, preceeded by other accessories (zircon, apatite, magnetite, see Fig. 2A, Petrík & Broska 1994) and a major part of plagioclase. Because these minerals either have very low LREE partitioning coefficients (plagioclase, biotite) or crystallize in very low abundances (zircon, apatite) they would not significantly influence the REE distributions of primary melt.

The presented results of SEM and microprobe study suggest strongly that the bright allanite domains escaped later oxidation and have, therefore, a primary composition. Since allanite REE partitioning coefficients (K_D^{All}) are known, it is possible to use them, along with the primary allanite compositions, to derive the REE composition of the parental granitoid magma precipitating the allanite. With K_Ds of Mahood & Hildreth (1983) the parental melt would display fractionated LREE abundances (with Sm/Nd ratio 0.11–0.16) significantly (1.5–3×) lower in LREE contents than the whole rock field (solid patern in Fig. 11). This may result from excesive values for distribution coefficients which were measured in highly polymerized high-silica rhyolites (l.c.). The use of K_Ds from less acid rocks, e.g. quartz latites (Chesner & Ettlinger 1989) would shift LREE abundances to the field defined by whole rocks but with the slope unchanged. Thus, the allanite data show that:

1 – The parental melt of the I-type granitoids was strongly LREE enriched with Sm/Nd ratio 0.11–0.16. The slope of such distribution seems to be steeper than that typical of possible crustal source lithologies (Sm/Nd = 0.17–0.20, McLennan 1990, dashed contour in Fig. 11). The steep slope of the parental melt suggests the role during melting, of a residual phase with high K_D for middle and heavy REE, such as garnet.

2 – The compositions of parental melts fall into the I-type tonalites field only when the lowest values of K_D^{All} are used (quartz latite 68 % SiO_2, Chesner & Ettlinger, l.c.) stressing the importance of parental melt major element composition for the right choice of a mineral K_D.

Conclusions

1 – The BSE study of allanite images revealed that they show a complicated internal zoning consisting of a patchwork of domains of variable brightness. The bright patches are interpreted as remnants of primary allanite, in contrast with later dark grey domains, which originated due to repeated interactions with late- to postmagmatic fluids. This is documented by textural relations between microcracks, voids and the replaced domains.

2 – Microprobe analyses characterize the Western Carpathian granitoid allanites as Ce-rich, relatively Al-poor and oxidated, particularly in darker patches. The last feature was identified by using a plot, total REE (+ Th + Y) vs. Al, contoured with F_{ox} isolines. The chemical variability of allanite can be interpreted in terms of substitutions (1, 2) leading to allanite ($Fe^{2+}Al$) and ferriallanite ($Fe^{2+}Fe^{3+}$) end-members.

3 – Two allanites measured by Mössbauer spectrometry have high F_{ox} ratios (0.48–0.53) which correlate well with the values read off the above plot. Primary allanite compositions follow the F_{ox} = 0.4 isoline suggesting that they may have been buffered through equilibration with biotite. This seems to be true

also for other igneous allanites. The published analyses from various other assemblages cover a wide compositional space defined by the quadrangle epidote - zoisite - allanite - ferriallanite.

4 - Comparison with Mössbauer-derived F_{ox} ratios of coexisting biotites showed that biotite maintains its F_{ox} values within a narrower range (15-17 % of Fe^{3+} of total Fe) compared to the range 35-55 in allanite. The oxidation effects included in Mössbauer data may account for the lack of direct correspondence between both ratios. Nevertheless, 40 % of the Fe^{3+} contained by primary allanite domains is believed to indicate the same fO_2 as do biotites with 15-17 % of Fe^{3+}.

5 - The REE distributions suggest a preferential escape of middle REE on interaction with late-stage fluids, but the overal REE mobility due to allanite oxidation is usually less than 20 % of the whole rock LREE content. The composition of granitoid parental melt crystallizing allanite, calculated using partitioning coefficients of Chesner & Ettlinger (1989), indicates that the parental melt was strongly LREE enriched, with a Sm/Nd ratio lower than that of the upper crust. This invokes the role of garnet in residual mineralogy.

Acknowledgment: Martin Radvanec is acknowledged for thoughtful reviews of earlier versions of the manuscript. This research was supported by grant GA 118 to I.P.

References

Broska I. & Gregor T., 1992: Allanite-monazite antagonism and magnetite-ilmenite granite series in the Tribeč Mts. *Spec. vol. IGCP* 276, 25-36.

Broska I. & Petrík I., 1993a: Tonalite of the Sihla-type (sensu lato): a Variscan plagioclase-biotite I-type magmatite in the Western Carpathians. *Miner. slovaca*, 25, 23-28 (in Slovak, English summary).

Broska I. & Petrík I., 1993b: Magmatic enclaves in granitoid rocks of the Western Carpathians. *Miner. slovaca*, 25, 104-108 (in Slovak, English summary).

Broska I. & Uher P., 1991: Regional typology of zircon and its relationship to allanite/monazite antagonism (on an example of Hercynian granitoids of Western Carpathians) *Geol. Carpathica*, 42, 5, 271-277.

Burt D.M., 1990: Compositional and phase relations among rare earth element minerals. In: Lipin B.R. & McKay G.A. (Eds.): *Geochemistry and mineralogy of rare earth elements. Reviews in Mineralogy*, 21, 259-307.

Cambel B., (Ed.), 1982: Preliminary results of integrated investigation of the selected samples of the West Carpathian granitoids. *Geol. Zbor. Geol. Carpath.*, 5, 33, 535-673.

Čech F., Vrána S. & Povondra P., 1972: A non-metamict allanite from Zambia. *Neu Jb. Min. Abh.*, 116, 208-223.

Chappel B.W. & White A.J.R., 1974: Two contrasting granite types. *Pacif. Geol.* 27, 173-174.

Chesner C.A. & Ettlinger A.D., 1989: Composition of volcanic allanite from the Toba tuffs, Sumatra, Indonesia. *Amer. Mineralogist* 74, 750-758.

Deer W.A., Howie R.A. & Zussman M.A., 1962: Rock-forming minerals. *Longmans*, London, 2nd. ed., 1-333.

Dollase W.A., 1971: Refinement of the crystal structures of epidote, allanite and hancockite. *Amer. Mineralogist*, 56, 447-464.

Droop G.T.R., 1987: A general equation for estimating Fe3+ concentrations in ferromagnesian silicates and oxides from microprobe analyses, using stoichiometric criteria. *Mineral. Mag.* 51, 431-435.

Exley R.A., 1980: Microprobe studies of REE-rich accessory minerals: Implications for Skye granite petrogenesis and REE mobility in hydrothermal systems. *Earth Planet. Sci. Lett.* 48, 97-110.

Fourcade S. & Allégre C.J., 1978: Trace element behavior in granite genesis: A case study the calc-alcaline plutonic association from the Querigut Complex (Pyrénées, France). *Contr. Mineral. Petrology*, 76, 177-195.

Grew E.S., Essene E.J., Peacor D.R., Su S.-C. & Asami M. 1991: Dissakisite-(Ce), a new member of the epidote group and the Mg analogue of allanite-(Ce), from Antarctica. *Amer. Mineralogist*, 76, 1990-1997.

Gromet L.P. & Silver L.T., 1983: Rare earth element distributions among minerals in a granodiorite and their petrogenetic implications. *Geochim. Cosmochim. Acta*, 47, 925-939.

Hovorka D., 1960: A contribution to petrography of Veporic granitoids (in Slovak with German abstract). *Acta geol. geogr. Univ. Comen., Geol.*, 4, 255-260.

Hovorka D., 1971: Orthite (allanite) from the Kohút crystalline complex. *Geol. Práce*, 147-163 (in Slovak).

Hovorka D. & Hvoždara P., 1965: Accesory minerals in Veporic granitoid rocks. Part I. *Acta geol. geogr. Univ. Comen., Geol.* 9, 145-179 (in Slovak, German summary).

Hvoždara P. & Határ J., 1978: Accesory minerals of some magmatic and metamorphic rocks of the Veporic unit. *Acta geol. geogr. Univ. Comen., Geol.*, 113-127 (in Slovak).

Kičinová D., 1992: Mössbauer spectroscopy in mineralogy. *Manuscript*, 1-64 (in Slovak).

Levinson A.A., 1966: A system of nomenclature for rare-earth minerals. *Amer. Mineralogist*, 51, 152-158.

Mahood G. & Hildreth W., 1983: Large partition coefficients for trace elements in high silica rhyolites. *Geochim. Cosmochim. Acta*, 47, 11-30.

McLennan S.M., 1990: Rare earth elements in sedimentary rocks: Influence of provenance and sedimentary processes. In: Lipin B.R. & McKay G.A. (Eds.): *Geochemistry and mineralogy of rare earth elements. Reviews in Mineralogy*, 21, 169-200.

Michael P.J., 1984: Chemical differentiation of the Cordillera Paine granite (southern Chile) by in situ fractional crystallization. *Contr. Mineral. Petrology*, 87, 179-195.

Noyes H.J., Wones D.R. & Frey A., 1983: A tale of two plutons: petrographic and mineralogical constraints on the petrogenesis of the Red Lake and Eagle Peak Plutons, central Sierra Nevada. *J. Geol.* 91, 353-379.

Peacor D.R. & Dunn P.J., 1988: Dollaseite-(Ce) (magnesium orthite redefined): Structure refinement and implications for F + M2+ substitutions in epidote-group minerals. *Amer. Mineralogist*, 73, 838-842.

Petrík I. & Broska I., 1989: Mafic enclaves in granitoid rocks of the Tribeč Mts., Western Carpathians: geochemistry and petrology. *Geol. Zbor. Geol. Carpath.* 40, 6, 667-696.

Petrík I. & Broska I., 1994: Petrology of two granite types from the Tribeč Mts., Western Carpathians: an example of allanite-magnetite vs. monazite-ilmenite dichotomy. *Geol. J.*, 29, 59-78.

Petrík I., Broska I. & Bezák V. 1993: A contribution to geochemistry and petrology of granitoids of the SW part of the Vepor unit. In: Rakús M. & Vozár J. (Eds.): *Geodynamic model and the deep structure of the Western Carpathians. GÚDŠ*, Bratislava, 207-218 (in Slovak, English abstract).

Petrík I., Broska I. & Uher P., 1994: Evolution of the Western Carpathian granite magmatism: age, source rock, geotectonic setting and relation to the Variscan structure. *Geol. Carpathica*, 45, 5, 283-291.

Sawka W.N. & Chappell B.W., 1988: Fractionation of uranium, thorium and rare earth elements in a vertically zoned granodiorite: Implications for heat production distributions in the Sierra Nevada batholith, California, U.S.A. *Geochim. Cosmochim. Acta*, 52, 1131-1143.

Sawka W.N., Chappell B.W. & Norrish K., 1984: Light -rare-earth-element zoning in sphene and allanite during granitoid fractionation. *Geology*, 12, 131-134.

Serdyuchenko D.P., 1980: Isomorphism in orthite. *Dokl. Akad. Nauk USSR*, 252, 126-128 (in Russian).

Sorensen S.S., 1991: Petrogenetic significance of zoned allanite in garnet amphibolites from a paleo-subduction zone: Catalina Schist, southern California. *Amer. Mineralogist*, 76, 589-601.

Spišiak J., Pitoňák P. & Caňo F., 1994: Allanite and Al-chromite from corundum-phlogopite rocks of the Jasenie - Kyslá area

(Nízke Tatry Mts.). *Miner. slovaca*, 26, 67-69 (in Slovak, English abstract).

Wones D.R. & Eugster H.P., 1965: Stability of biotite: experiment, theory and application. *Amer. Mineralogist*, 50, 1228-1272.

Zakrzewski M.A., Lustenhouwer W.J., Nugteren H.J. & Williams C.T., 1992: Rare-earth minerals yttrian zirconolite and allanite-(Ce) and associated minerals from Koberg mine, Bergslagen, Sweden. *Mineral. Mag.* 56, 27-35.